TECHNICAL REPORT: ANTIPROTON-PROTON ANNIHILATION AT REST INTO $K^{\circ}_{L}K^{\pm}\pi^{\mp}\pi^{\circ}$

Castulus Kolo
University of Munich

Munich, 23. August 1995

1 Introduction

This CB-note is a summary of the analysis of $\bar{p}p \to K^\circ_L K^\mp \pi^\pm \pi^\circ$ at rest in liquid hydrogen [1]. It outlines the data selection including particle identification and kinematic fitting as well as the partial wave analysis of 14234 events.

2 Software

For data production and Monte Carlo studies the following software was used:

- GEANT version 3.1590
- CBGEANT version 4.06/07
- CBOFF version 1.22/02
- CBKFIT version 2.09/07

3 Data Selection

The ideal signature of a $K^\circ_L K^\mp \pi^\pm \pi^\circ$ event are two tracks in the JDC, two unmatched PED's resulting from the π° decay and missing energy due to the K°_L and the $K^\pm$, which is at first interpreted as a pion in data reconstruction. The charged pion and kaon respectively can be identified from their differential energy loss in the JDC.

Yet in most of the cases this signature is obscured because of 'hadronic split-offs' and a possible K°_L-interaction. Both processes lead to additional unmatched PED's. Therefore we selected events with 2 to 4 unmatched PED's to increase the available statistics.

3.1 The Data

The analysis of the $K^\circ_L K^\mp \pi^\pm \pi^\circ$ final state is based on the following data sets given in table 1. To define the final state topology several preselection cuts were applied:

Table 1: Preselection cuts and number of surviving events:

Run period	June 1991	August 1991	November 90
Trigger	2 prong	2 prong	min. bias
Total number of events	2200595	2340240	4291507
Two long vertex tracks ($\sum q_i = 0$)	1567539	1674096	867665
$\sum E_i \leq 1600$ MeV	216522	221870	145907
2 PED's (*unmatched*)	33981	34871	22355
3 PED's (*unmatched*)	41946	43498	27100
4 PED's (*unmatched*)	42533	43950	29771
$\sum$ 2-4 PED's ($K^\circ_L K^\mp \pi^\pm \pi^\circ$)	118460	122319	79226

The cut on the total energy $\sum E_i$ (IEHDCB(13)) is chosen as to acount for the K_L° either missing or leaving only part of its energy in the calorimeter and for the misinterpretation of the charged kaon as a pion. Figure 1 shows the distribution of the total energies for selected events (after the kinematic fit). The distribution for 'ideal' events with only 2 PED's is smeared out to higher energies in the case of 3 and 4 PED events. This is due to hadronic split offs and K_L°-interaction.

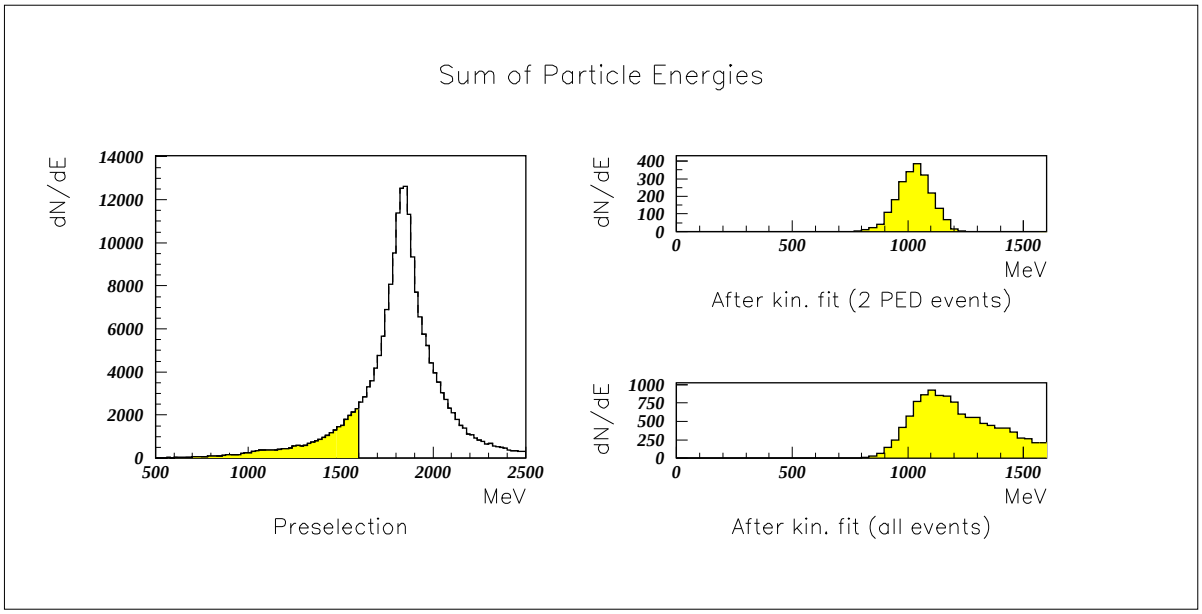

Figure 1: Left: Sum of particle energies and applied preselection cut. Right: Distribution of the total energy for selected events. In the case of 2 PED-events the values are well below 1600 MeV. In the corresponding distribution for all (2-4 PED's) events, less then 5 % are discarded due to the cut.

After the preselection further cuts were applied to increase the data quality:

Table 2: Further cuts to increase the data quality and the number of discarded events in each step (N_{PED}^{total} = unmatched + matched PED's):

Run period	June 1991	August 1991	November 90
Events after preselection (2-4 PED's)	118460	122319	79226
No dE/dx values in TTKS bank	288	343	990
PED in Xtal 13	12303	15641	14084
$N_{PED}^{total} - N_{tracks} < 2$	821	844	496
Remaining number of events	105048	105491	63656

3.2 Identification of Charged Pions and Kaons

The distribution of the dE/dx values versus the total momenta is shown in figure 2. The two bands of pions and kaons are clearly visible. A third and presumable even a fourth one appears only for positive particles. The latter match with the expected bands of protons and deuterons respectively.

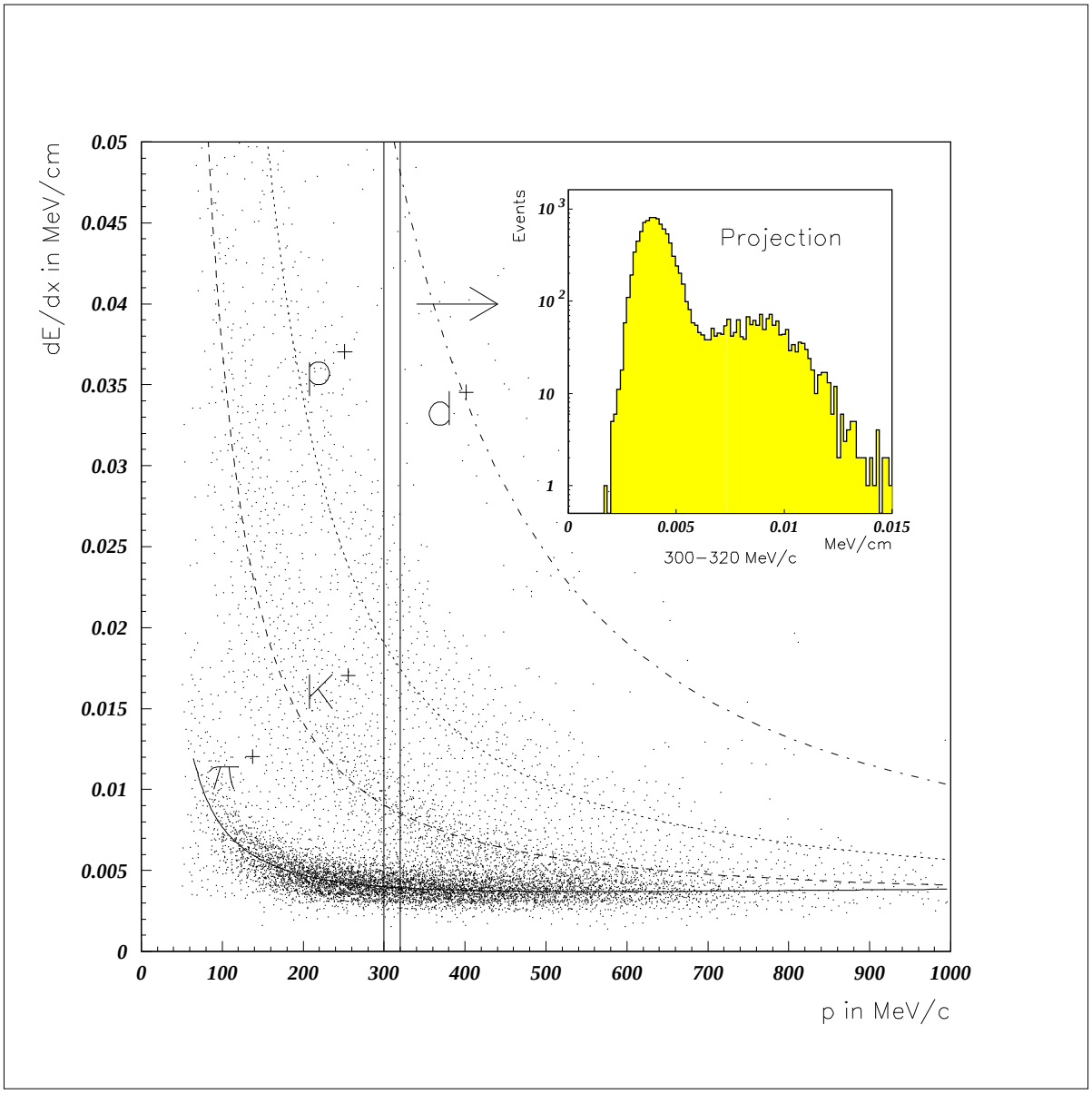

Figure 2: Distribution of the differential energy loss versus the momenta for positively charged particles (June 91).

In order to compare the data with the theoretically expected Bethe-Bloch function the momentum space is cut into slices of 20 MeV/c. One would expect the sum of two Landau shaped distributions. However due to the applied truncated mean method [2] and the limited dE/dx and momentum resolution they can be aproximated with two gaussians (figure 3). The projections of dE/dx were fitted for all momentum slices over the relevant range, and the resulting values for sigma and mean plotted against β (figure 4).

To match the Bethe Bloch function with the data it was corrected by multiplying it with a third order polynomial. The behaviour of σ varying with β was parametrised by the following function: $\sigma = f(\beta) = a \cdot e^{b/\beta} + c$ (for $\beta > d$) and $\sigma = f'(d) \cdot (\beta - d) + f(d)$ (for $\beta \leq d$). The two times (for dE/dx and σ) four coefficients (a, b, c, d) were fitted separately for the three different run periods and Monte Carlo.

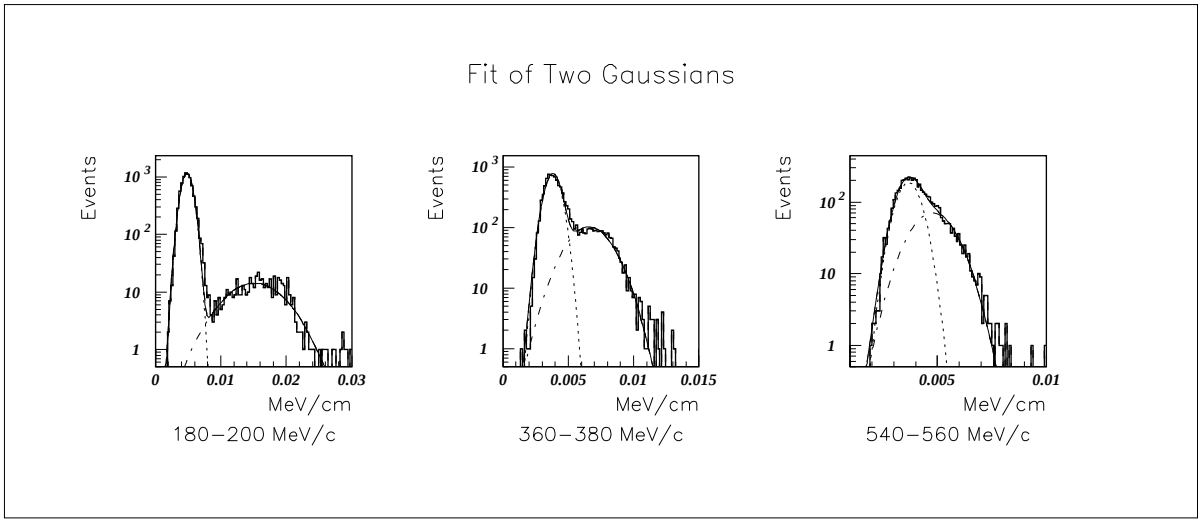

Figure 3: Fit of two gaussians to the dE/dx distribution for three different momentum ranges.

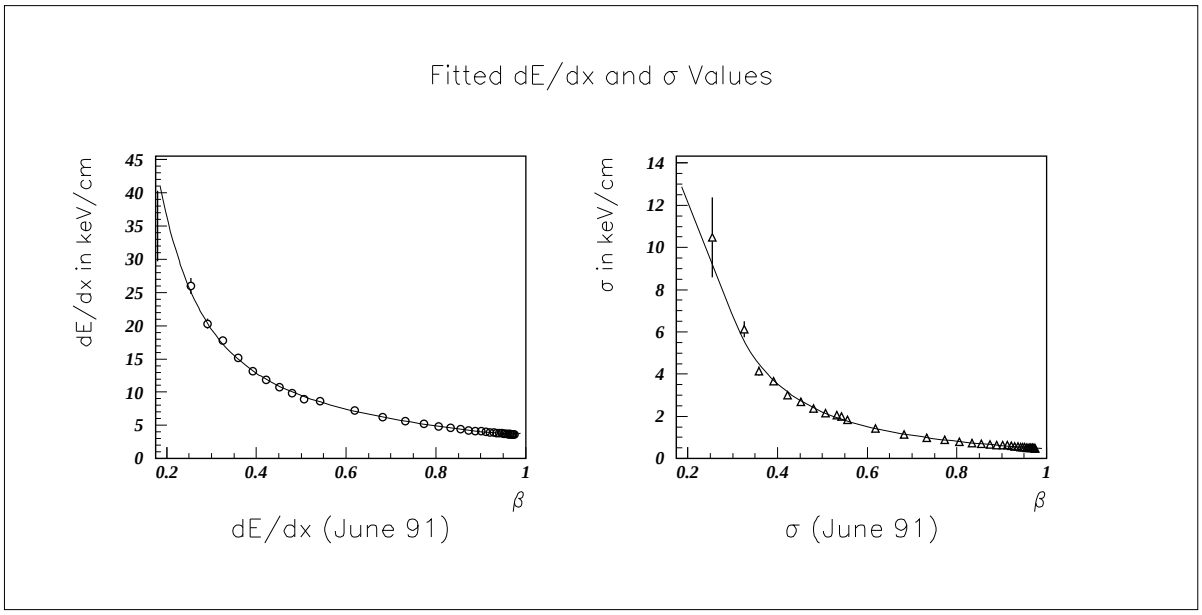

Figure 4: Fitted functions for the June 91 data. Left: Corrected Bethe Bloch function. Right: Sigma. The values up to $\beta = 0.5$ are obtained for kaons, above that for pions.

With these sets of coefficients for each run period the theoretically expected mean value of $\overline{(dE/dx)}_{\pi^\pm/K^\pm}$ and $\sigma_{\pi^\pm/K^\pm}$ respectively can be calculated for a given momentum under the asumption of the particle either beeing a pion or a kaon. Hence the normalised distances of the measured $(dE/dx)_{exp.}$ to the two mean values are:

$$d_{\pi^\pm} = \frac{(dE/dx)_{exp.} - \overline{(dE/dx)}_{\pi^\pm}}{\sigma_{\pi^\pm}} \tag{1}$$

and

$$d_{K^\pm} = \frac{(dE/dx)_{exp.} - \overline{(dE/dx)}_{K^\pm}}{\sigma_{K^\pm}} \tag{2}$$

The following procedure was used to define the particle identity:

- IF ($d_{K^\pm} \geq 3$) THEN proton or deuteron ($\rightarrow$ discard event);
- ELSE IF ($d_{K^\pm} \geq -1$) THEN kaon;
- ELSE IF ($d_{\pi^\pm} \leq 2$) THEN pion;
- ELSE no identification possible ($\rightarrow$ discard event).

The areas in the dE/dx versus momentum plane corresponding to the applied cuts are displayed[1] in figure 5.

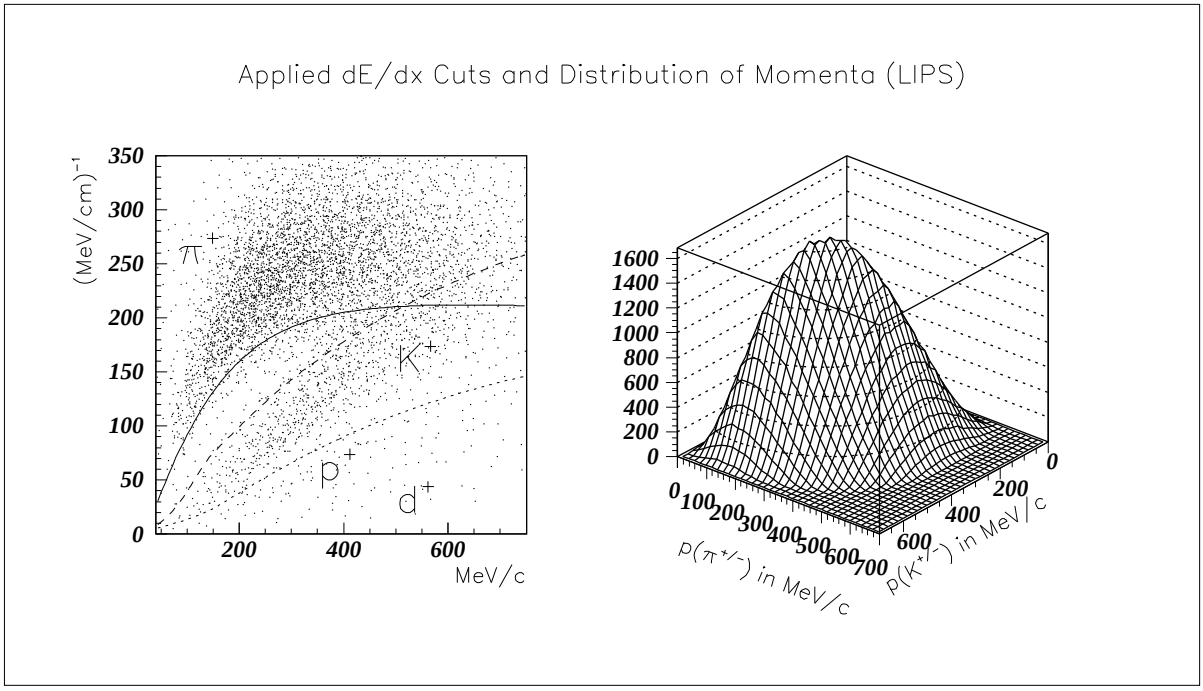

Figure 5: Left: Distribution of $(dE/dx)^{-1}$ with all three cut parameters (solid line: $d_{\pi^\pm} = 2$, broken line: $d_{K^\pm} = -1$, dotted line: $d_{K^\pm} = 3$). Right: phase space distribution of the particle momenta (LIPS).

For momenta of more than 520 MeV/c this assignment becomes ambigous. However the fraction of $K^\circ_L K^\mp \pi^\pm \pi^\circ$ events with pions in this momentum region is less than 2% (fig. 5). In addition for such events the probability of the kaon having a momentum less than 450 MeV/c is more than 95 %. That is for approximately all $K^\circ_L K^\mp \pi^\pm \pi^\circ$ events there is at least one particle in a momentum region were it is safely identified.

However there are other events such as $\pi^+\pi^- + X$ or $K^+K^- + X$ misinterpreted as $K^\circ_L K^\mp \pi^\pm \pi^\circ$ events. The smallness of their feedthrough after all subsequent cuts (including kinematic fit) can be judged by comparing the distributions of the normalised distances $d_{K^\pm}$ and $d_{\pi^\pm}$ before the dE/dx cut with those of finally selected events (fig. 6). In the latter case both can be described (approximately) by symmetric gaussians (a quantitative estimation of the residual background is given in section 3.6).

[1] By plotting 1/(dE/dx) instead of dE/dx the minimum ionizing region, where pion and kaon band merge, is displayed in a better way.

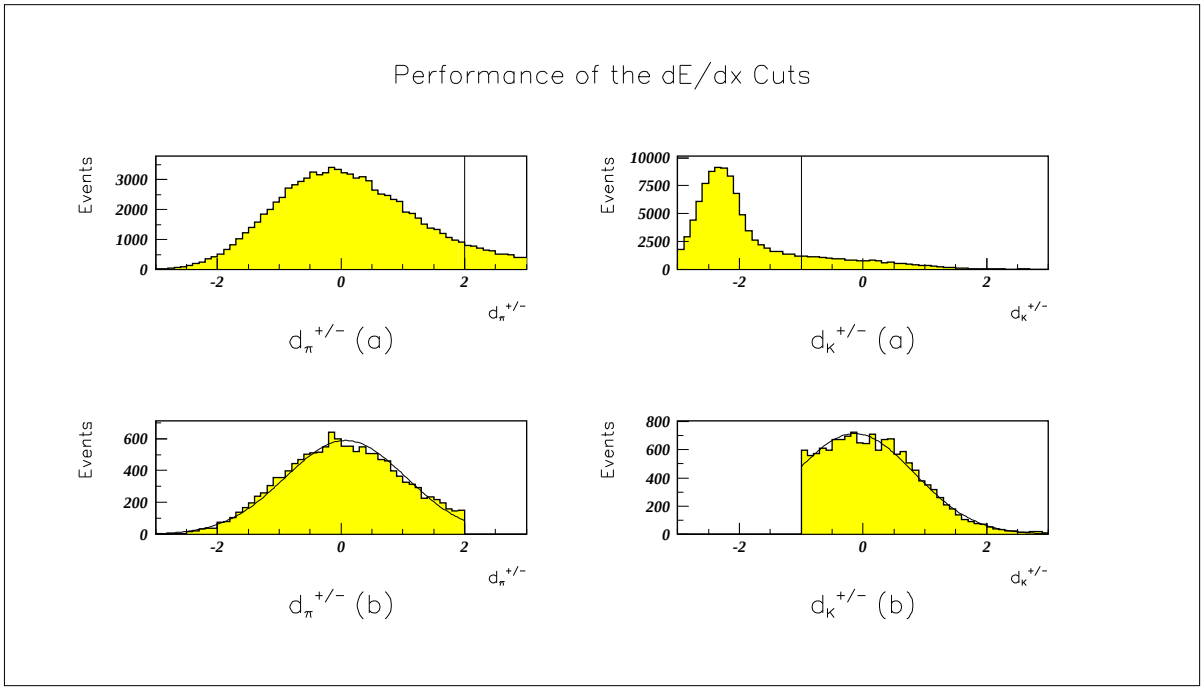

Figure 6: Distribution of the normalised distances before the dE/dx cut (a) and for finally selected events after the kinematic fit (b).

Another qualitative impression of the goodness of this cut is given by the distribution of invariant masses:

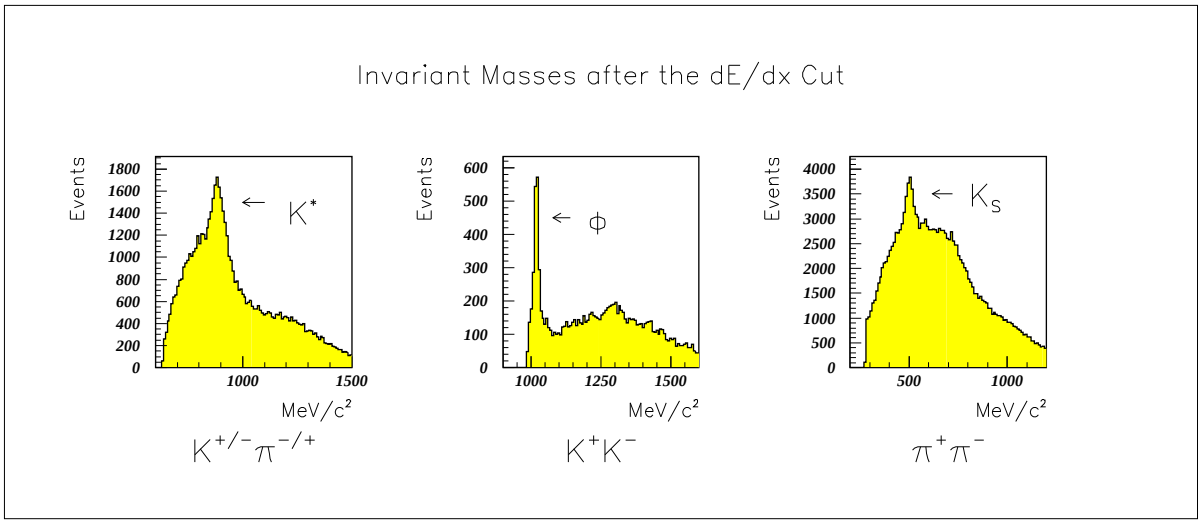

Figure 7: Distributions of invariant masses after assignment by the dE/dx criterion. Already at this stage of the selection process the expected resonant states are clearly visible.

The applied dE/dx cut has the following properties:

- For all momenta an equal fraction of events is discarded. The original momentum distribution is therefore not distorted. The efficiency over the whole phase space is equally distributed.
- This procedure is independent of the absolute values of dE/dx and σ. It can be transferred easily to other run periods and Monte Carlo.

- By variation of only two parameters ($d_{\pi_\pm}$, $d_{K_\pm}$) the cuts are easy to optimize or to change to more restrictive values.

The efficiency for $K^\pm\pi^\mp$ events has been proved with Monte Carlo studies to be aproximately constant at 70% (see figure 6b).

Only $K^\pm\pi^\mp$-events were passed on to the subsequent steps of the data selection (see table 5 for a summary of the selection statistics).

3.3 π° and K_L° Mass Window

Due to hadronic split offs and K_L° interaction in most of the cases there are more than the two unmatched PED's from the π° decay. The following method was used to reconstruct the π°:

- Try all possible two PED combinations and check if at least one of these are in the required mass window from 110 to 160 MeV/c^2 (fig. 8). If so, then continue.

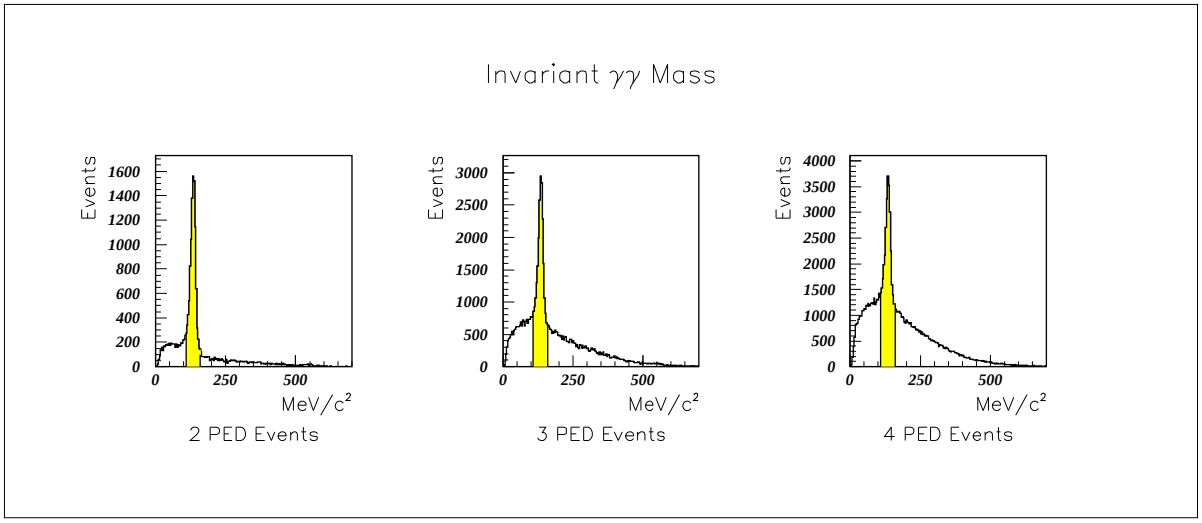

Figure 8: The invariant $\gamma\gamma$ mass subdivided for events with different numbers of unmatched PED's (preselected events after identification of charged particles).

- Check if the missing mass calculated under this hypothesis is in the required range from 500 to 600 MeV/c^2 (fig. 9). If so, then store this combination.
- All such combinations are than fed into the kinematic fit. In case of more then one successful fit, only the best combination is used for further analysis. If the second best combination has a confidence level greater than 0.1 the event is discarded. This anti cut avoids ambiguities.

Events with two, three and four unmatched PED's were analysed in this way. For the finally selected events the 'spare' PED's can be attributed either to a hadronic split off or a K_L° interaction ([1], appendix C, p. 177).

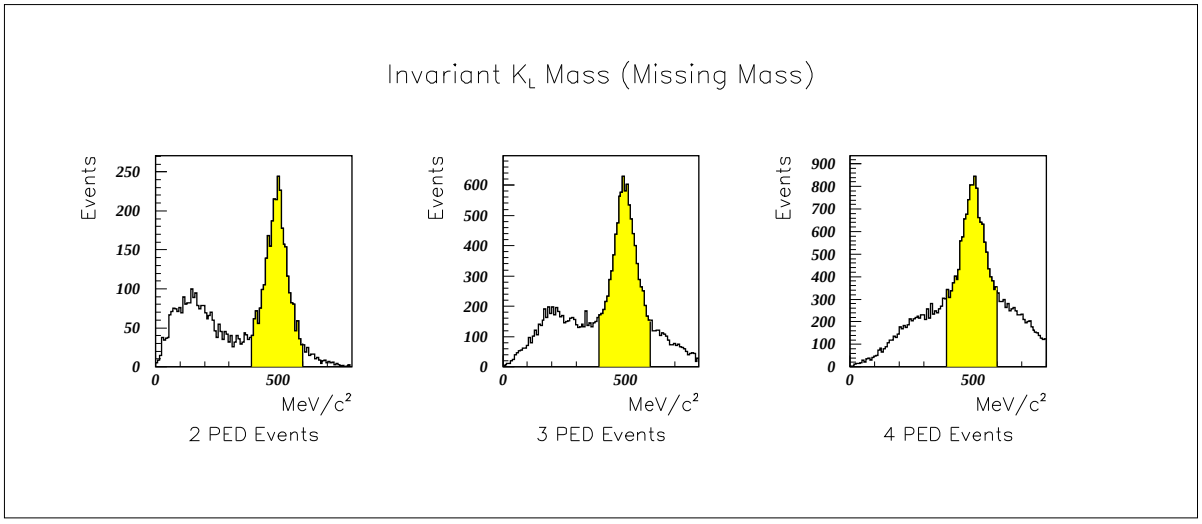

Figure 9: The invariant K_L° mass (missing mass) subdivided for events with different numbers of unmatched PED's (preselected events after identification of charged particles).

3.4 Kinematic Fit

For all events with at least one combination of two PED's fullfilling the above mentioned criteria a 2C kinematic fit (CBKFIT) was applied:

$$\sqrt{(E_{K_L^\circ})^2 - (\vec{p}_{K_L^\circ})^2} = m_{K_L^\circ}$$

$$\sqrt{(E_{\pi^\circ})^2 - (\vec{p}_{\pi^\circ})^2} = m_{\pi^\circ}$$

In order to achieve proper pulls the standard errors for the kinematic fit and the momenta for the charged particles in the TTKS banks were corrected [3]:

```
Q(JTTKS+46) = Q(JTTKS+46) * b**2
Q(JTTKS+47) = Q(JTTKS+47) * a * b
Q(JTTKS+48) = Q(JTTKS+48) * a**2
Q(JTTKS+49) = Q(JTTKS+49) * b * c
Q(JTTKS+50) = Q(JTTKS+50) * a * c
Q(JTTKS+51) = Q(JTTKS+51) * c**2
```

where a,b,c are given in table 3.

Table 3: Correction factors used for this analysis:

charged particles			PED's		
a	b	c	a	b	c
2.34	1.44	1.00	1.43	1.43	1.37

Table 4: Correction factors for the momenta of charged particles:

(+)	(-)
1.055	1.045

The distribution of the resulting pulls is shown in figure 10.

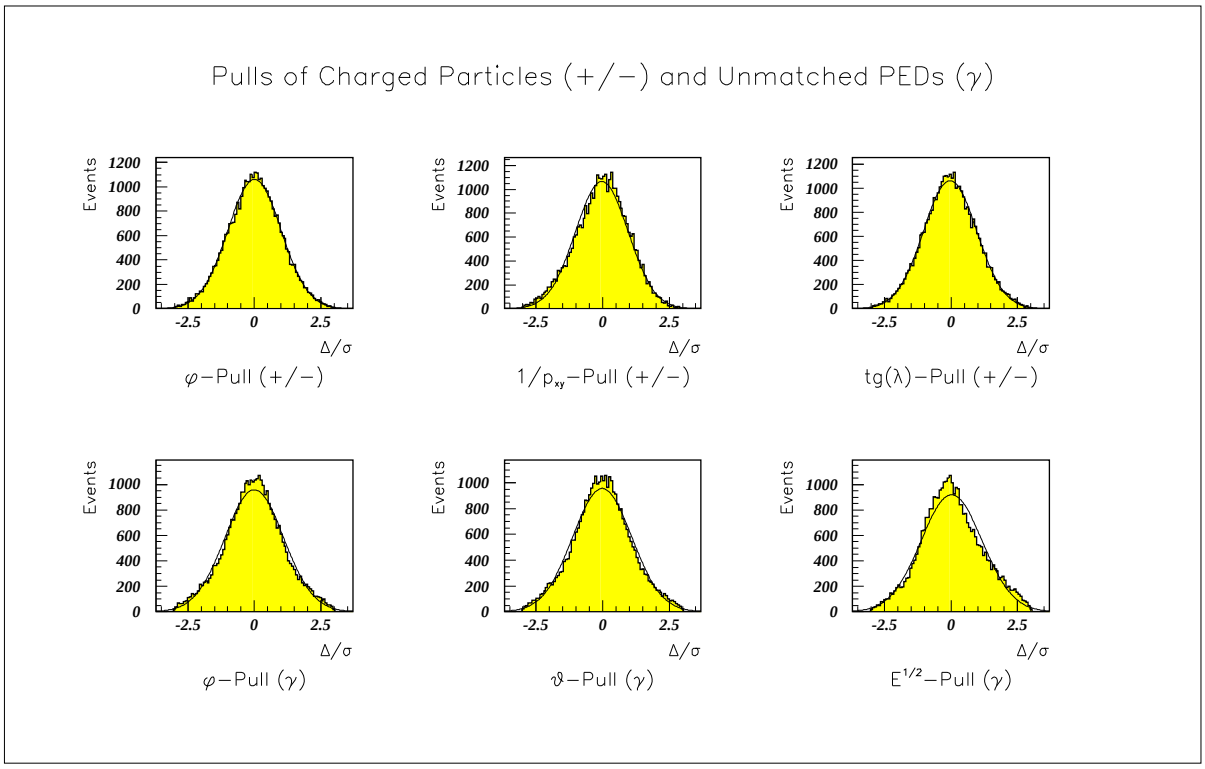

Figure 10: Pulls of charged particles (+/−) and unmatched PED's (γ).

For each of the three data sets (2, 3 and 4 PED events) a different confidence level cut (fig. 11) was chosen.

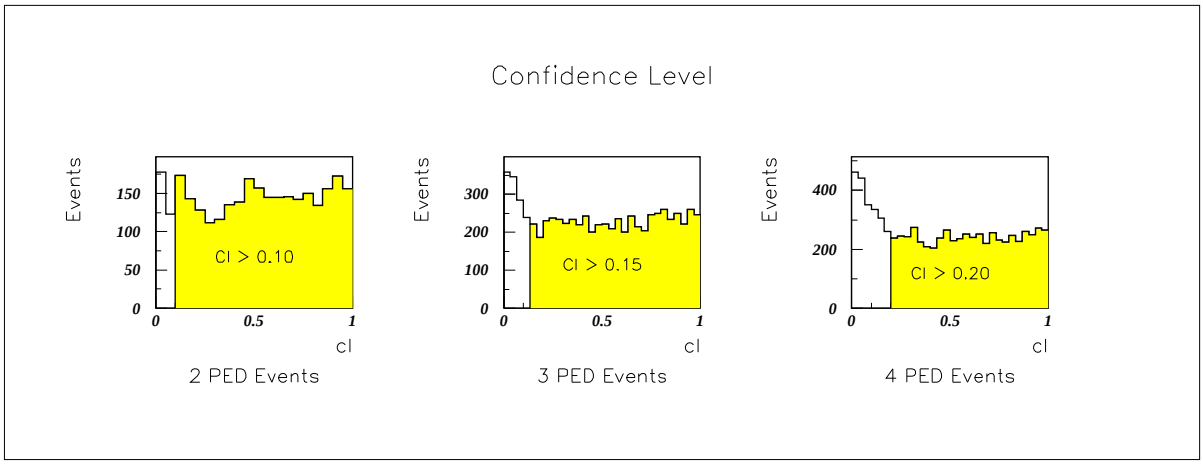

Figure 11: The distribution of confidence levels above the chosen thresholds is flat.

An anti cut on the second best combination (if there is any) and the $K^\circ_L K^\circ_S \pi^\circ$ hypothesis ($K^\circ_S \to \pi^+\pi^-$) avoids ambiguities and reduces background, respectively.

The effect of all applied cuts is summarised in table 5.

Table 5: Effect of the different cuts to select the final state $K^\circ_L K^\mp \pi^\pm \pi^\circ$:

Run period	June 1991	August 1991	November 90
events after preselection	105048	105491	63656
Identification of charged particles (dE/dx)			
K^+K^-	5290	4368	3270
$\pi^+\pi^-$	65464	68712	39454
proton or deuteron	1180	2200	372
no identification possible	9680	9092	4616
$K^\pm\pi^\mp$	23434	21119	15944
Reconstruction of the π° and the K°_L			
no good 2-PED-combination	14565	13538	11257
Kinematic fit			
no convergence	329	261	213
Confidence-level-cut	1550	1369	892
Further cuts to reduce background			
second best comb. (cl$\geq$ 0.1)	807	681	454
$K^\circ_S K^\circ_L \pi^\circ$ hyp. (cl$\geq$ 0.01)	106	106	135
remaining number of events	6077	5164	2993
subdivided according to the number of unmatched PED's			
2-PED events	1179	960	481
3-PED events	2397	2098	1215
4-PED events	2502	2106	1297
Sum of all remaining $K^\circ_L K^\mp \pi^\pm \pi^\circ$ events: 14234			

3.5 Invariant Mass Spectra

Projections of a 5-dimensional variable space always lead to a loss of information. Furthermore their interpretation is difficult due to possible interferences. However some features discussed in the section on the partial wave analysis are also apparent in the following diagrams.

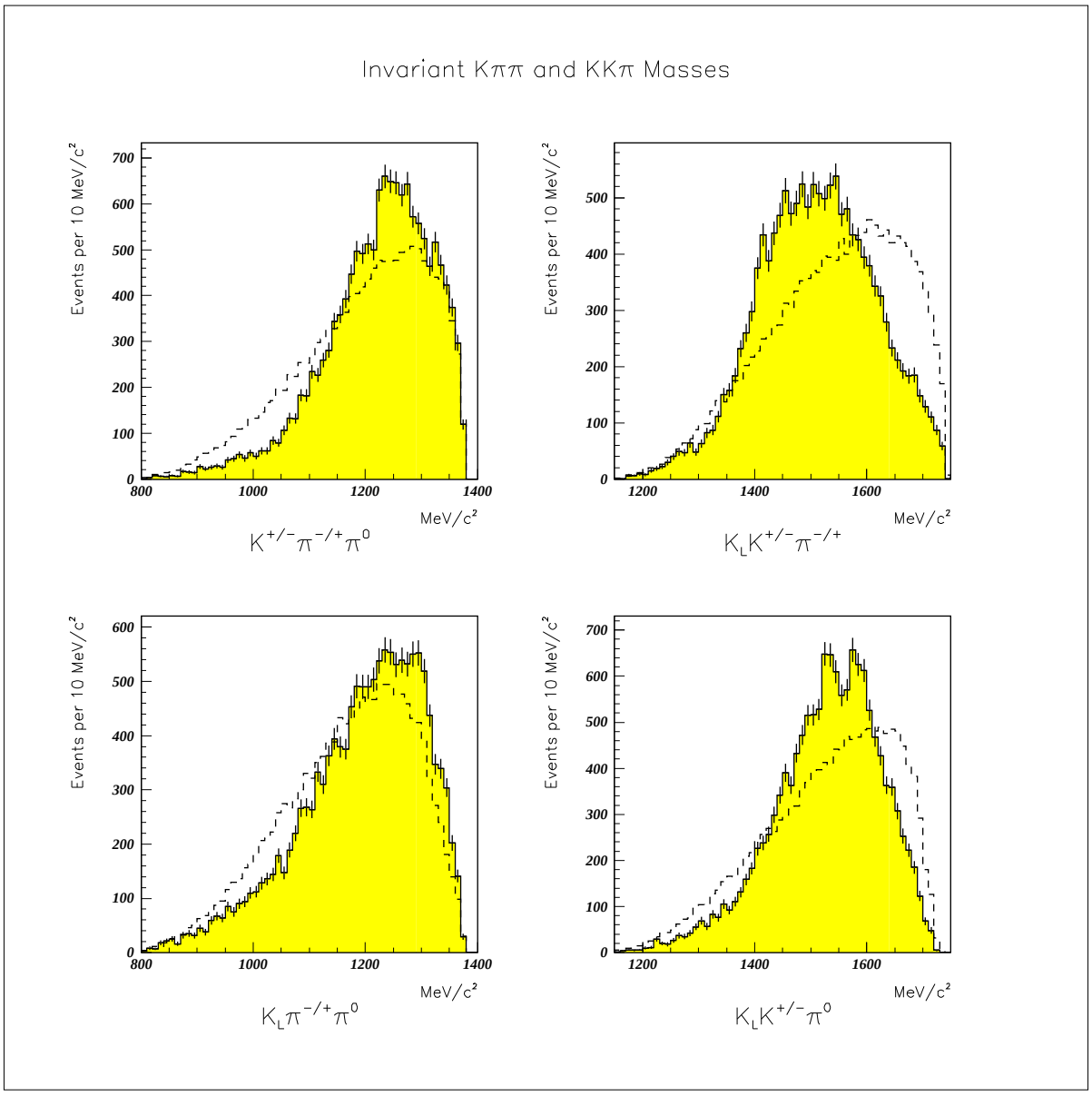

Figure 12: Distributions of the invariant $KK\pi$ and $K\pi\pi$ masses for the charged (bottom) and neutral (top) combination. Real data (shaded histograms) and phase space distributed Monte Carlo events (superimposed histograms).

- There is a strong asymmetry between the charged and the neutral $K\pi$, $\bar{K}K\pi$ and $K\pi\pi$ spectra.
- In the $K^{\circ}_{L}K^{\pm}\pi^{\circ}$ system there are two narrow signals at masses of 1530 and 1585 MeV/c^2. A considerable fraction of decays into the final state $K^{\circ}_{L}K^{\mp}\pi^{\pm}\pi^{\circ}$ proceeds via $K^{*}(890)$ resonances (fig. 13).

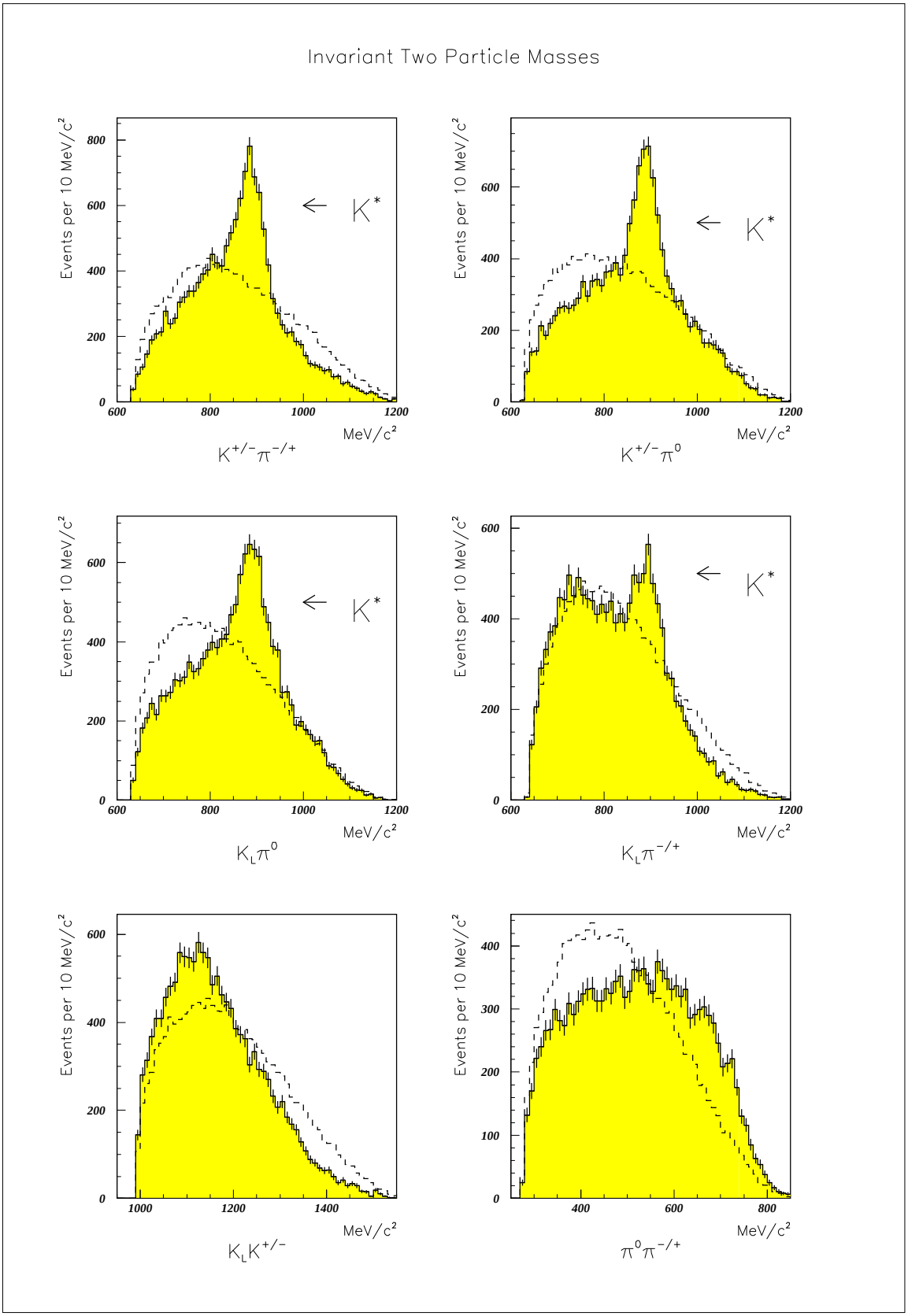

Figure 13: Invariant mass distributions of all possible two particle combinations for real data (shaded histograms) and phase space distributed Monte Carlo events (superimposed histograms).

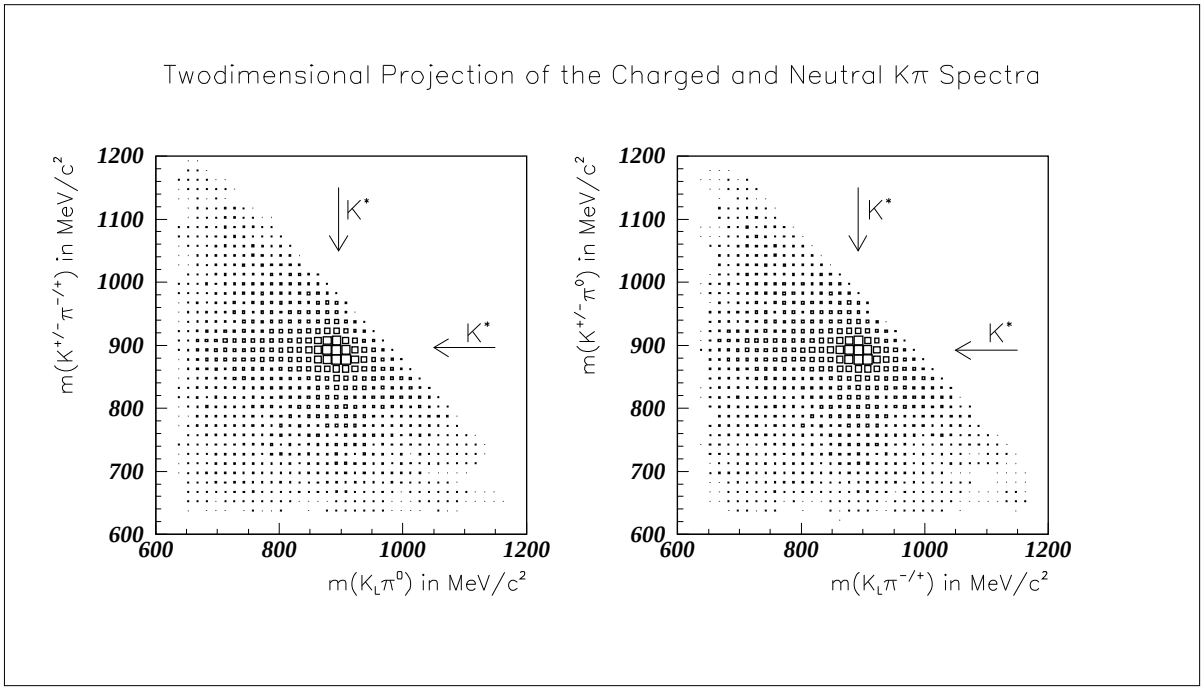

Figure 14: The twodimensional projection of the charged and neutral $K\pi$ spectra underlines the importance of contributions: $\bar{p}p \to \bar{K}^*K^*$.

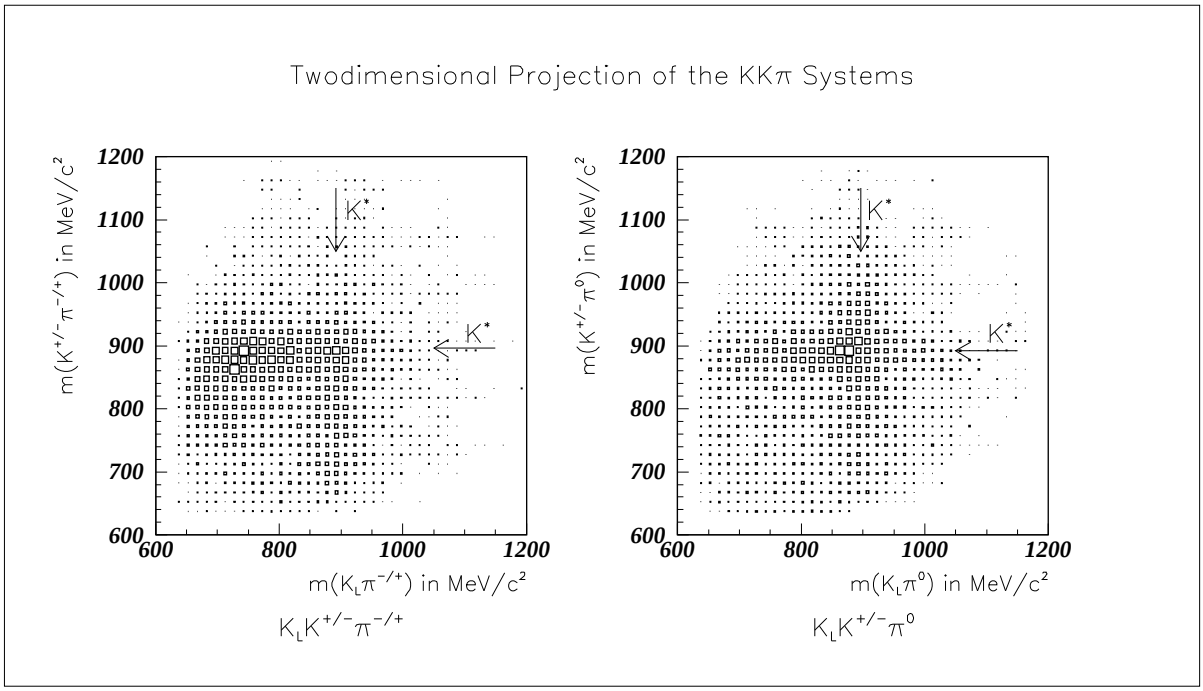

Figure 15: The two-dimensional projection of the $KK\pi$ systems.

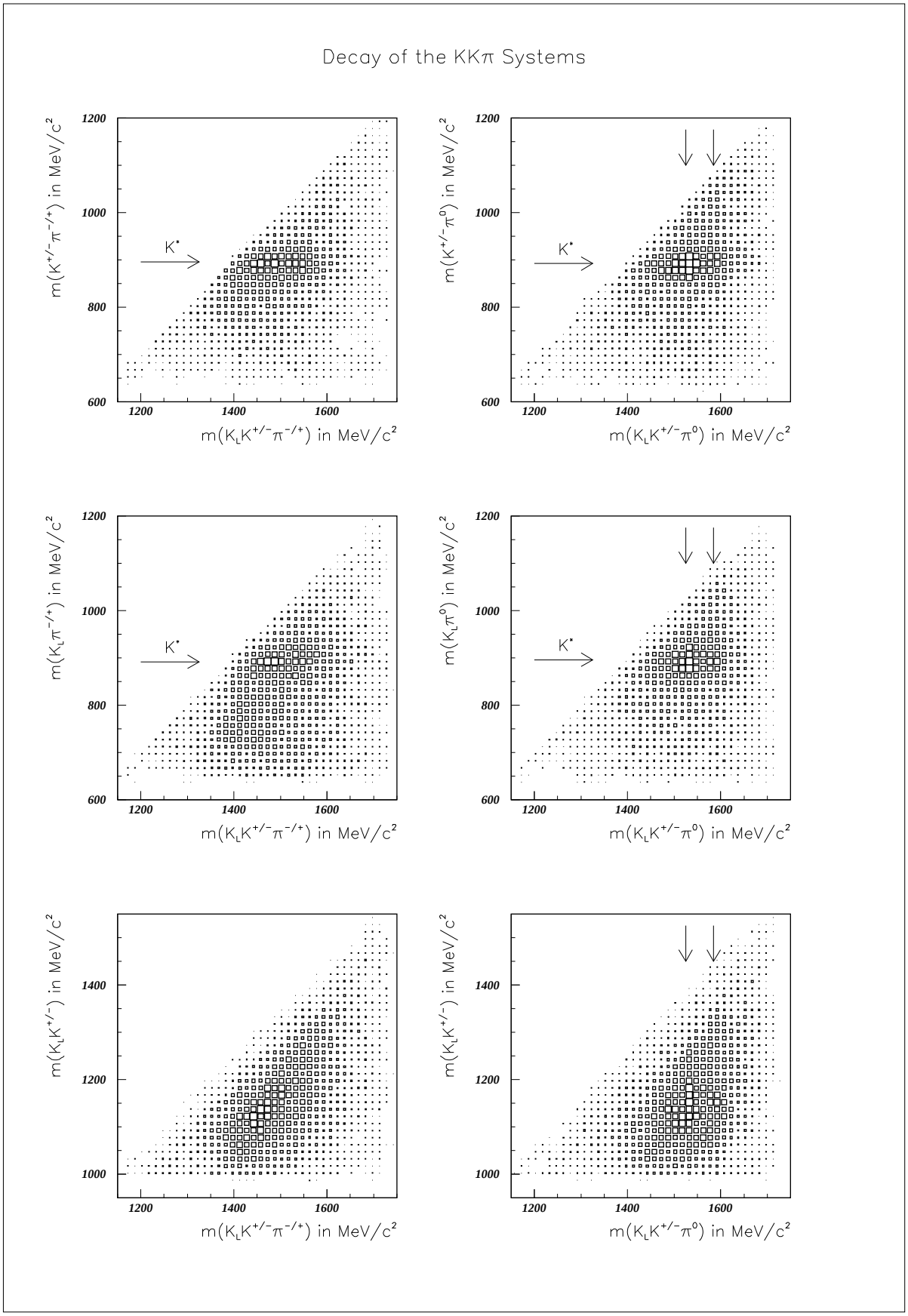

Figure 16: The twodimensional projection of the invariant $K\pi$ masses versus the $KK\pi$ masses indicates decays via K^*K. The structures in the $\bar{K}K$ versus $\bar{K}K\pi$ diagramms are reflections thereof. The arrows indicate the positions of the narrow peaks in the $K^0_L K^{\pm}\pi^{\circ}$ invariant mass spectrum (fig. 12).

3.6 Estimation of Residual Background:

The main sources of background are:

(i) The applied dE/dx cut to select $K^{\pm}\pi^{\mp}$ events is a compromise between the two requirements of high statistics and best possible reduction of K^+K^-+X and $\pi^+\pi^-+X$ events. Therefore some feedthrough will remain.

(ii) Due to the cut on the total energy not only K°_L events but also others with a particle either missing or not depositing all of its energy in the spectrometer are enriched. However in the distribution of the directions of reconstructed K°_L momenta there is no indication of a significant contribution of such events:

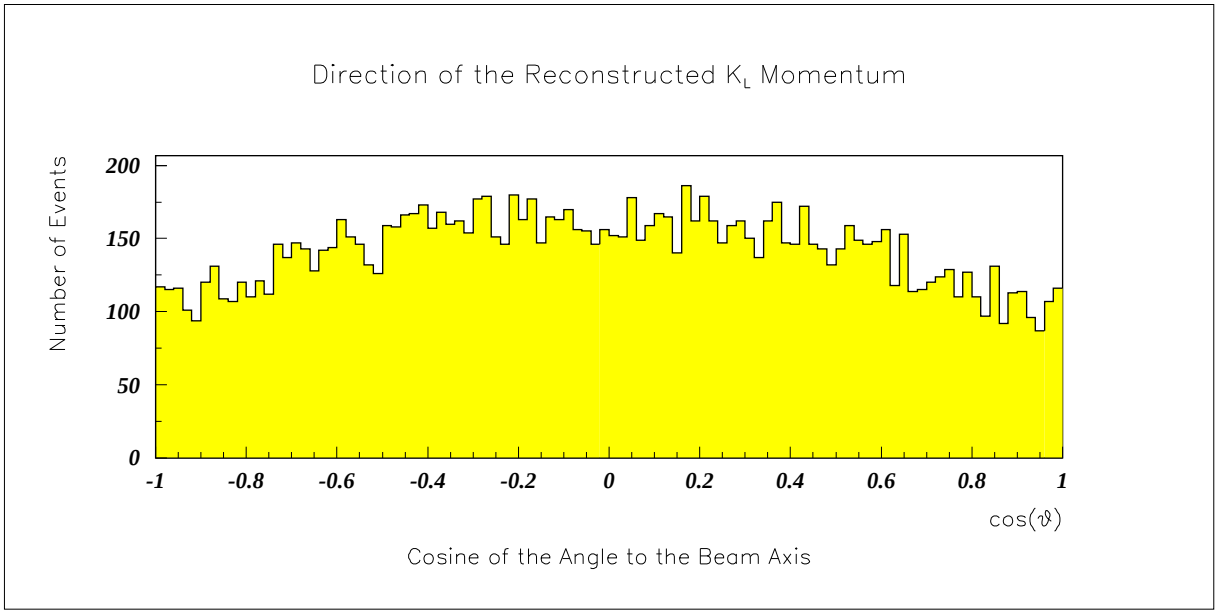

Figure 17: The distribution of the direction of K°_L momenta shows no significant rise at $cos(\vartheta) = \pm 1$

(iii) For the selection of the final state $K^{\circ}_L K^{\mp}\pi^{\pm}\pi^{\circ}$ events with 2, 3 and 4 PED's were analysed. Apart from the two unmatched PED's of the π° decay there is a surplus of up to two 'spare' PED's. Hence in some cases there is more than one possible combination to reconstruct a π° and a K°_L in the corresponing mass range. The fraction of wrongly reconstructed π° was tested with Monte Carlo events. The applied cuts reduce their contribution to $< 1\%$. The actual number depends thereby on the Monte Carlo (structure and probability of K°_L interaction and hadronic split-offs). Any significant influence of such events on the shape of the invariant mass spectra and the partial wave analysis respectively could be excluded by comparing the three data sets for different numbers of unmatched PED's (see for example fig. 18).

(iv) A K°_L interaction and hadronic split offs can lead to two unmatched PED's, which by mistake could be interpreted as arising from a π°. For the reaction $\bar{p}p \to K^{\circ}_L K^{\pm}\pi^{\mp}$ the feedthrough has been tested to be less than 1% (actual number depending on Monte Carlo). In this case again the comparison of the data sets with 2, 3 and 4 unmatched PED's ruled out an eventual influence on the results of the analysis.

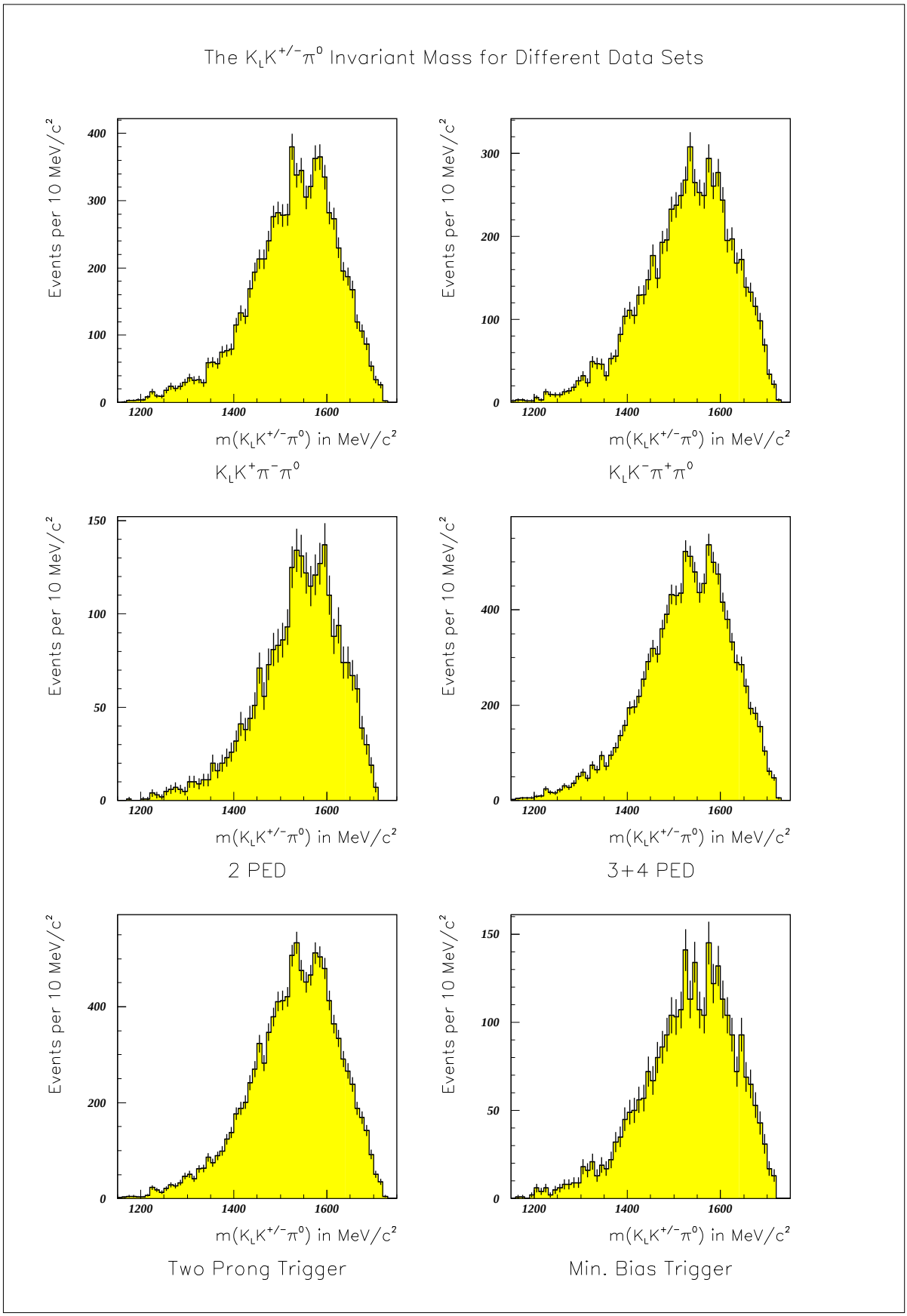

Figure 18: The invariant $K_L^\circ K^\pm \pi^\circ$ mass for different data sets.

Hence there are various sources of background each contributing with a small fraction. The sum can be estimated from the distribution of the missing mass for finally selected events but with the unfitted values of the fourmomenta (fig. 19):

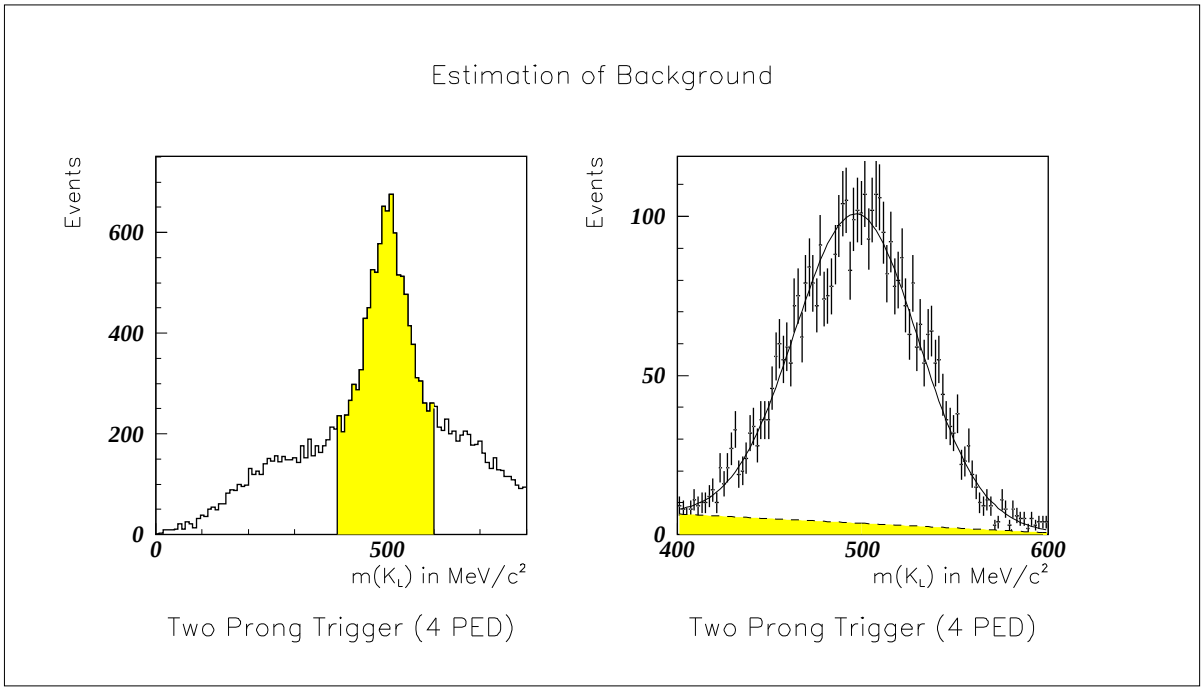

Figure 19: Estimation of the background contribution.

This was done separately for the data sets of different run periods and numbers of unmatched PED's. The background under the K_L° signal before the kinematic fit (figure 19 left) is due to combinatorics and feedthrough of wrong events. After all selection cuts the K_L° signal should be of gaussian shape. However this is not exactly the case (figure 19 right). A fit with a gaussian on a linear background yields a value of

$$\frac{background}{number\,of\,all\,events} \approx (11 \pm 3)\,\%$$

as average over all data sets.

The background contribution is mainly due to a misinterpretation of the charged particles. This can be seen from the distributions of the normalised distances to the mean value of the kaon and the pion band respectively. In the distribution of the pion band there is a surplus of events on top of the expected gaussian distribution towards the kaon band. The same is the case for the kaon band. Counting these events leads to a number of $10 \pm 2\%$ which is consistent with the value above.

The influence of this kind of background can be controlled by setting the dE/dx cut to more restrictive values: For example the cut value of $d_{K^\pm}$ from -1. to -0.5 or the one of $d_{\pi^\pm}$ from 2. to 1. (figure 21).

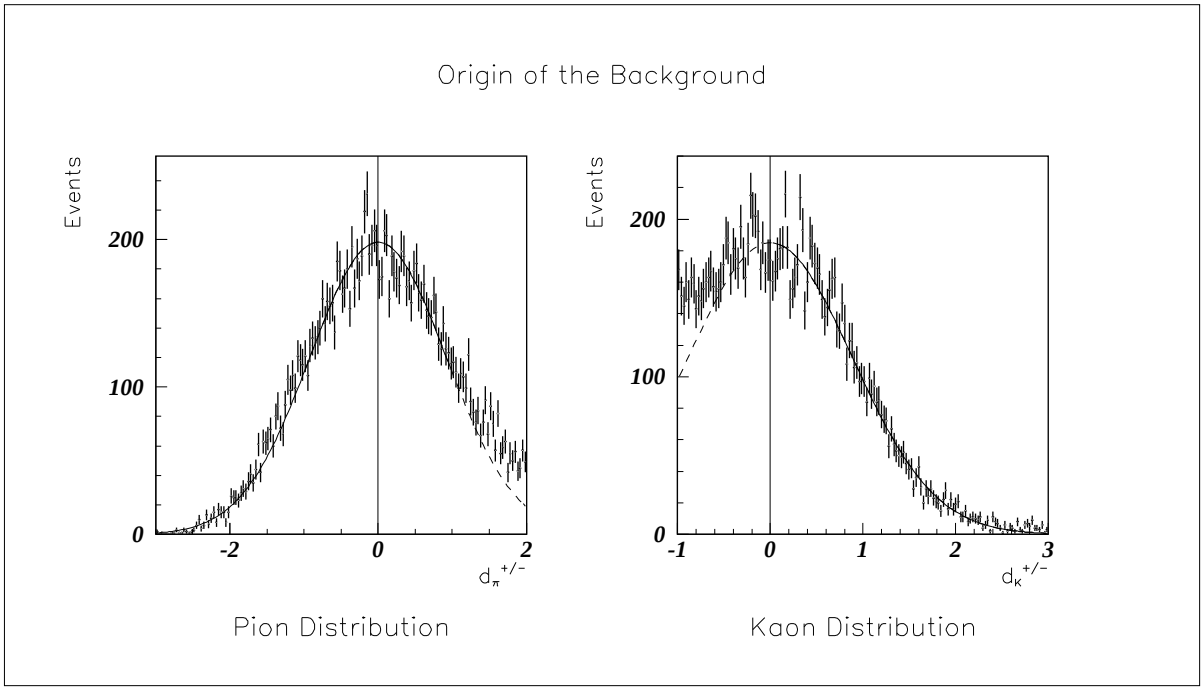

Figure 20: Wrongly identified pions and kaons show up as an enhancement on top of the expected gaussian distribution.

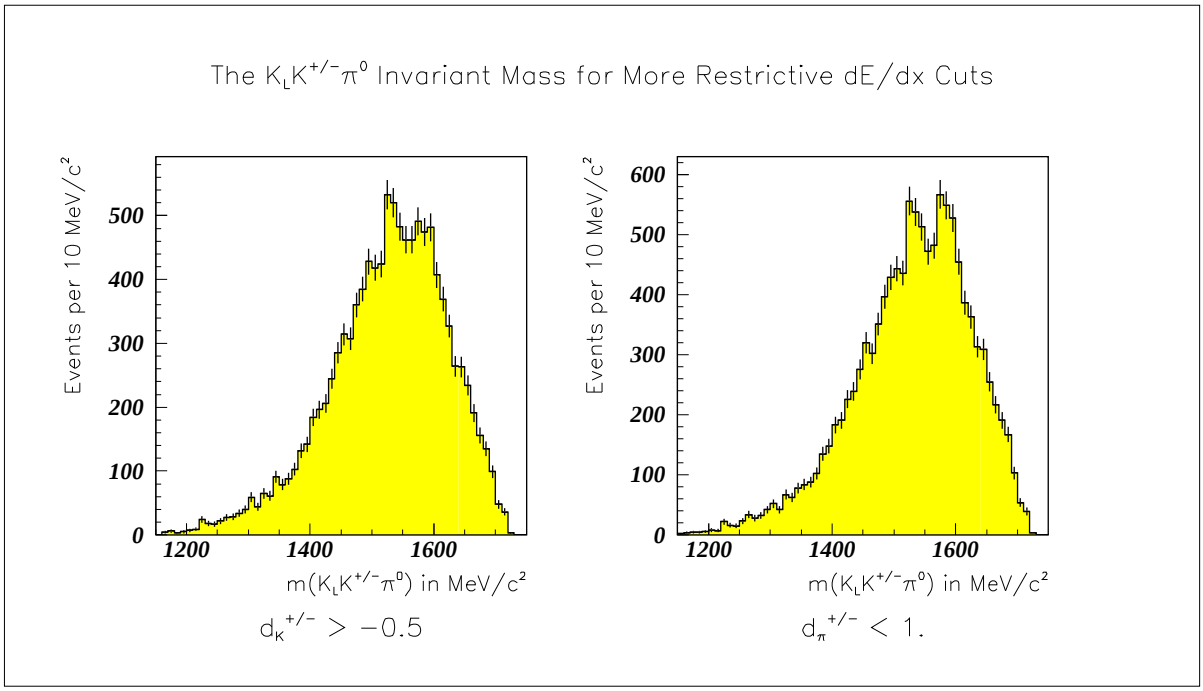

Figure 21: A more restrictive cut on the normalised distances to the mean values of the kaon or pion band does not significantly change the features of the spectra. The example of the $K_L^\circ K^\pm \pi^\circ$ spectrum was chosen to demonstrate this fact.

3.7 Monte-Carlo

Corrections for acceptance variations and limited resolution were evaluated by a Monte Carlo calculation based on phase space distributed $K^\circ_L K^- \pi^+ \pi^\circ$ and $K^\circ_L K^+ \pi^- \pi^\circ$ events.

A principal problem of the Monte Carlo available at the time of this analysis was the simulation of hadronic interactions with the calorimeter [4], in particular the K°_L interaction [5]. The Monte Carlo results were compared for four different conditions:

Table 6: Monte Carlo efficiencies under different conditions:

	$K^\circ_L K^- \pi^+ \pi^\circ$	$K^\circ_L K^+ \pi^- \pi^\circ$
0% K°_L interaction	$(16.8 \pm 0.1)\%$	$(15.8 \pm 0.1)\%$
100% K°_L interaction	$(6.7 \pm 0.1)\%$	$(5.1 \pm 0.1)\%$

The unequal efficiencies are due to the differences in the number and kind of hadronic interactions and therefore in the number of events with 2, 3 and 4 unmatched PED's Apart from the different Monte Carlo efficiencies for these four data sets, the momentum and invariant mass distributions for events which passed the data selection process are in all cases identical.

Assuming the interaction probability of the K°_L to be 50% [5], the overall Monte Carlo efficiency can be derived from the numbers given in table 6:

$$\text{Monte Carlo efficiency} \quad = \quad (11.1 \pm 0.2)\ \%$$

as the average of all four data sets.

For the partial wave analysis a sample of 60000 Monte Carlo events was used.

4 Partial Wave Analysis

4.1 Method

The partial wave analysis was performed in the full 5-dimensional space of kinematic variables. The helicity formalism [6] [7] was used for a description of the angular dependence of the amplitudes, which were restricted to be two-particle states. In terms of the isobar-model [8], the initial $\bar{p}p$ system is assumed to decay to the $K_L^\circ K^\mp \pi^\pm \pi^\circ$ final state through a series of quasi two-body decays. In the helicity formalism, an isobar of spin J decays into two daughters of spin S_1 an S_2. They have total spin S and relative angular momentum L. The spin dependence of the transition can be written as a matrix [9][10]:

$$\mathcal{A}(J;LS) = \mathcal{D}^J_{\lambda,m}(\theta,\phi) \cdot \ < J\lambda|LS0\lambda >< S\lambda|S_1S_2\lambda_1,-\lambda_2 > \times F_L(q) \times \mathcal{BW}_L(m). \quad (3)$$

The matrix has $(2S_1+1)(2S_2+1)$ rows and $(2J+1)$ columns. The row index $\lambda = \lambda_1 - \lambda_2$ runs over all possible final state helicities, while the column index m runs over the magnetic substates of the isobar. In the rest frame of the isobar, q is the final state momentum, while θ and ϕ refer to the decay angles. The final amplitude or weight for the current event is obtained by taking the trace of the transition matrix and multiplying this number by the phase space weight[2]. F_L is the damping factor, and $\mathcal{BW}_L$ is the Breit-Wigner amplitude for the isobar decay. The damping or penetration factors $F_L(q)$ are given by [11]:

$$\begin{aligned} F_0(q) &= 1 \quad (4)\\ F_1(q) &= \sqrt{\frac{2z}{z+1}} \\ F_2(q) &= \sqrt{\frac{13z^2}{(z-3)^2+9z}} \end{aligned}$$

where

$$z = (q \cdot R)^2 = \left(\frac{q[MeV/c]}{197,3}\right)^2 \quad (5)$$

The Breit-Wigner factors are given by [12]

$$\mathcal{BW}(m) = \frac{m_0\Gamma_0}{m_0^2 - m^2 - i \cdot m_0\Gamma(m)} \quad (6)$$

where

$$\Gamma(m) = \Gamma_0 \frac{m_0}{m}\frac{q}{q_0}\frac{F_L^2(q)}{F_L^2(q_0)} \quad (7)$$

with m_0 and Γ_0 the nominal mass and width of a resonance and q_0 the corresponding decay momentum.

For the $K\pi$ S-wave, the results of LASS [13] were used. The elastic $K\pi$ phase shift was read of their figure 15; it was put to zero below 0.8 GeV/c^2.

[2]Acceptance corrections are absorbed in the phase space weight.

The quantum numbers of the $\bar{p}p$ system for a given decay are restricted by parity and C-parity conservation. For meson-antimeson pairs ($\bar{K}^*K^*$) there are further restrictions due to Bose-symmetry. The amplitudes, corresponding to established particles (1a-4e), which were considered[3] in the fits are given in table 7.

Table 7: Possible primary decays of the $\bar{p}p$ system and the corresponding angular momenta. B: forbidden by Bose-symmetry, P: forbidden by parity conservation, C: forbidden by C-parity conservation (only in case of neutral decay products).

Decays into the $K_L^\circ K^\mp\pi^\pm\pi^\circ$ final state S: Total Spin of the decay products				$\bar{p}p$ initial state (J^{PC})					
				S-wave		P-wave			
Type	Nr.	Decay	S	0^{-+}	1^{--}	1^{+-}	0^{++}	1^{++}	2^{++}
$(K\pi)+(\bar{K}\pi)$	1a	$K^*(892)+\bar{K}^*(892)$	0	P	1	P	0	P	2
	1b	$K^*(892)+K^*(892)$	1	1	B	0,2	P	B	B
	1c	$K^*(892)+K^*(892)$	2	P	1	B	2	2	0,2
	1d	$(K\pi)_s+K^*(892)$	1	P	0	1	1	1	1
	1e	$(K\pi)_s+(K\pi)_s$	0	P	1	P	0	P	2
$(K\pi\pi)+\bar{K}$	2a	$K_1(1270)+K$	1	P	0,2	1	1	1	1
	2b	$K_1(1400)+K$	1	P	0,2	1	1	1	1
	2c	$K^*(1410)+K$	1	1	1	0,2	P	0,2	2
	2d	$K_2^*(1430)+K$	2	2	2	1	P	1	1
$(K_L^\circ K^\pm)+(\pi^\mp\pi^\circ)$	3	$a_0(980)+\rho(770)$	1	P	0	1	1	1	1
$(K\bar{K}\pi)+\pi$	4a	$0^{-+}(\eta)+0^{-+}$	0	P	C	C,P	0	P	2
	4b	$1^{++}(f_1)+0^{-+}$	1	P	C	C	1	1	1
	4c	$1^{+-}(h_1,\ b_1)+0^{-+}$	1	C,P	0,2	1	C	C	C
	4d	$1^{--}(\phi)+0^{-+}$	1	C	1	0,2	C,P	C	C
	4e	$2^{-+}(\pi_2)+0^{-+}$	2	P	C	C	2	2	0,2
	4f	$0^{--}+0^{-+}$	0	C,P	1	P	C	C,P	C
	4g	$1^{-+}+0^{-+}$	1	1	C	C	P	0,2	2
	4h	$2^{++}+0^{-+}$	2	2	C	C	P	1	1
	4i	$2^{+-}+0^{-+}$	2	C	2	1	C,P	C	C
	4j	$2^{--}+0^{-+}$	2	C,P	1	2	C	C	C

The nominal masses and width of the particles are taken from the particle data group [14]. For the secondary decay of the K_1 resonances the following possibilities were tried in the fits:

$$K\pi\pi \ \rightarrow \ K^*(892) \ + \ \pi \tag{8}$$

$$K\pi\pi \ \rightarrow \ \rho(770) \ + \ K \tag{9}$$

$$K\pi\pi \ \rightarrow \ (K\pi)_s \ + \ \pi \tag{10}$$

For the $K^*(1410)$ and the $K_2^*(1430)$ only the first two amplitudes are allowed by parity conservation. For the decay of resonances in the $\bar{K}K\pi$ systems the two amplitudes:

$$K\bar{K}\pi \ \rightarrow \ K^*(892) \ + \ K \tag{11}$$

[3]In more detail for 4a-e the following resonances were considered: $\eta(1295)$, $\eta(1440)$, $f_1(1285)$, $f_1(1420)$, $f_1(1510)$, $h_1(1380)$, $b_1(1235)$, $\varphi(1680)$, $\pi_2(1670)$.

$$K\bar{K}\pi \;\rightarrow\; a_0(980) \;+\; \pi \tag{12}$$

were considered in the fits. In addition to known particles, also others were introduced in the analysis (4f-4j). The background is approximated by incoherent phase space distributed Monte Carlo events.

The data are subjected to an unbinned maximum likelihood fit [15] over the full 5-dimensional $K^{\circ}_{L}K^{\mp}\pi^{\pm}\pi^{\circ}$ phase space, using the MAXTOOL [16] software package[4]. The dynamic weights were normalized by Monte Carlo events which had to pass the same acceptance cuts as the experimental data.

The fits can be compared on the basis of their difference in the likelihood $\mathcal{L}$. The quality of the fits was judged by a comparison of the $\bar{\chi}^2/_{d.o.f}$ of the one-dimensional projections of all invariant mass combinations.

4.2 Results

The quantity of amplitudes (table 7) together with the fact that for all decays over K resonances (amplitudes 1a-2d) and for the decay via the $I = 1$ $\bar{K}K\pi$ resonances (some of the amplitudes 4a-j) there exists a neutral and a charged version renders a simultaneous fit with all possible partial waves unfeasible. However by comparing the results of a large number of variations a kind of 'minimal model' could be developed. That is a model with the minimum number of amplitudes wich are necessary to reach a reasonable description of the data.

Amplitudes of the Type: $\bar{p}p \rightarrow (K\pi) + (\bar{K}\pi)$

In a first naive model (model 0) only the following amplitudes from S-wave annihilations were considered:

$$\bar{p}p(1^{--}) \;\xrightarrow{S=0,\,L=1}\; K^{*\circ} \;+\; \bar{K}^{*\circ} \qquad neutral \tag{13}$$

$$\bar{p}p(1^{--}) \;\xrightarrow{S=0,\,L=1}\; K^{*+} \;+\; K^{*-} \qquad charged \tag{14}$$

$$\bar{p}p(1^{--}) \;\xrightarrow{S=2,\,L=1}\; K^{*\circ} \;+\; \bar{K}^{*\circ} \qquad neutral \tag{15}$$

$$\bar{p}p(1^{--}) \;\xrightarrow{S=2,\,L=1}\; K^{*+} \;+\; K^{*-} \qquad charged \tag{16}$$

$$\bar{p}p(1^{--}) \;\xrightarrow{L=1}\; (K\pi)^{\circ}_{s} \;+\; (\bar{K}\pi)^{\circ}_{s} \qquad neutral \tag{17}$$

$$\bar{p}p(1^{--}) \;\xrightarrow{L=1}\; (K\pi)^{+}_{s} \;+\; (K\pi)^{-}_{s} \qquad charged \tag{18}$$

$$\bar{p}p(0^{-+}) \;\xrightarrow{S=1,\,L=1}\; K^{*\circ} \;+\; \bar{K}^{*\circ} \qquad neutral \tag{19}$$

$$\bar{p}p(0^{-+}) \;\xrightarrow{S=1,\,L=1}\; K^{*+} \;+\; K^{*-} \qquad charged \tag{20}$$

[4]MAXTOOL is a partial wave analysis tool using the MINUIT minimization package [17] [18] [19] and an updated version of SPIN [9].

This model yields $\mathcal{L} = 3051$ and $\bar{\chi}^2/_{d.o.f.} = 4.46$. The most obvious discrepancies between the fit and real data are in the $K\pi$ invariant mass spectra. The number of K^* is not well reproduced. Therefore it is necessary to introduce further amplitudes with such intermediate states.

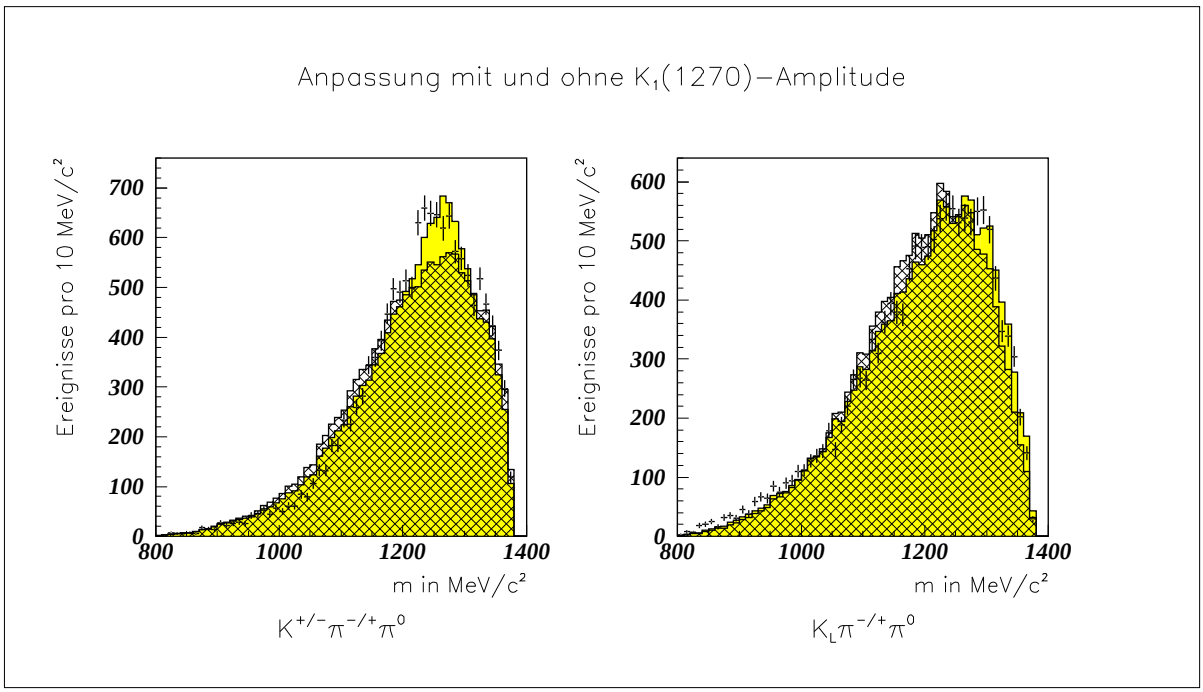

Figure 22: The dark histograms represent the results of model 0. The charged $K\pi\pi$ spectrum is aproximately reproduced. In the neutral $K\pi\pi$ spectrum an enhancement at 1270 MeV/c^2 becomes obvious. The introduction of the neutral decay $\bar{p}p(1^{--}) \stackrel{L=0}{\rightarrow} K_1^\circ(1270)+K_L^\circ$ und $K_1^\circ(1270) \stackrel{\ell=0}{\rightarrow} K^*(892)+\pi$ improves the fit considerably (grey histograms).

Amplitudes of the Type 2: $\bar{p}p \rightarrow K + (\bar{K}\pi\pi)$

Figure 22 underlines the importance of K_1 amplitudes. In an upgrade of model 0 the amplitudes

$$\begin{aligned} \bar{p}p(1^{--}) \stackrel{L=0}{\rightarrow} \quad & K_1(1270) \quad + K \\ & K_1(1270) \stackrel{\ell=0}{\rightarrow} K^*(892) \; + \; \pi \\ & K_1(1270) \stackrel{\ell=1}{\rightarrow} (K\pi)_s \; + \; \pi \\ & K_1(1270) \stackrel{\ell=0}{\rightarrow} \rho(770) \; + \; K \end{aligned} \tag{21}$$

were introduced separately for the charged:

$$\bar{p}p \rightarrow K_1^{\mp}(1270)K^{\pm}$$

and the neutral version:

$$\bar{p}p \rightarrow K_1^\circ(1270)K_L^\circ.$$

Figure 23 left shows the improvement of the fit with varying $K_1(1270)$ mass. A simultaneous fit of the $K_1^\circ(1270)$ mass and width yields:

Table 8: Result of a simultaneous fit of the $K_1^\circ(1270)$ mass and width on the base of model 0 and the addition of the neutral decay $\bar{p}p(1^{--}) \to K_1^\circ(1270)K_L^\circ$ (values in MeV/c^2).

Resonance	Mass m	Decay Width $\Gamma_\circ$
$K_1^\circ(1270)$	1274 ± 2	91 ± 7

For the charged version $\mathcal{L}$ also varies slightly with the mass but there is no clear maximum at $m_{K_1^\pm(1270)} = 1270$ MeV/c^2.

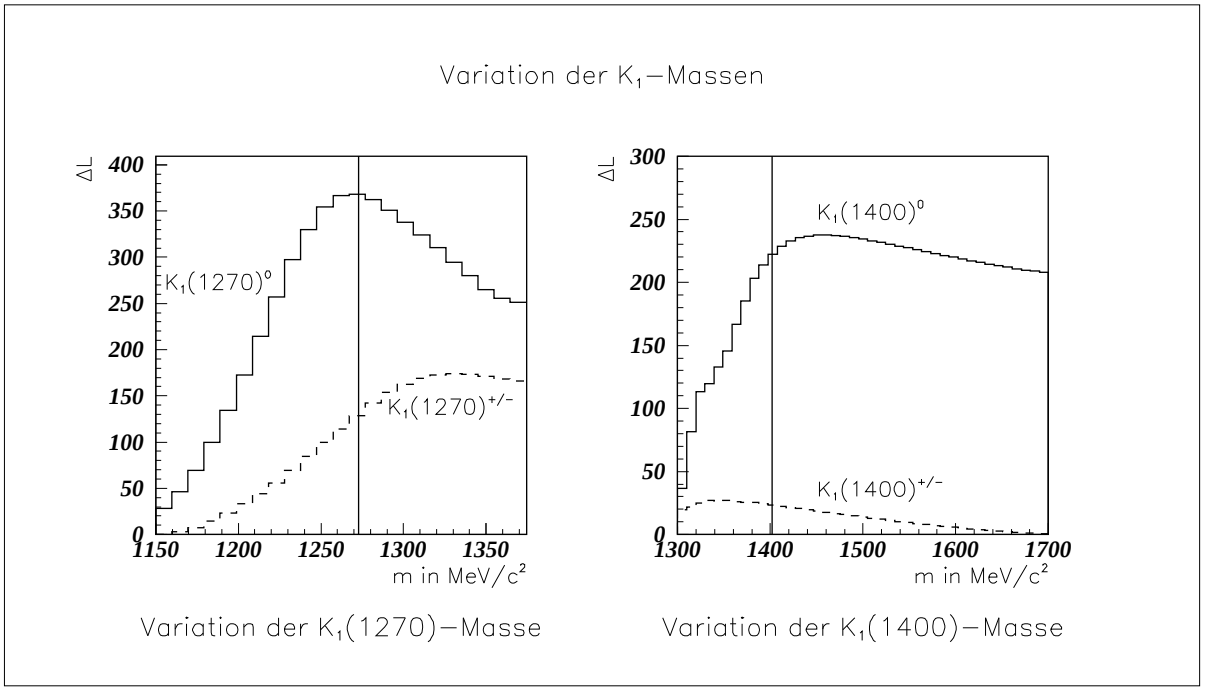

Figure 23: The change of $\mathcal{L}$ (ΔL in the figure) under variation of the K_1 masses (width as in [14]). The addition of decays over $K_1(1270)$ and $K_1(1400)$ to model 0 improves the fit significantly only for the neutral version.

In the same way a possible contribution of the $K_1(1400)$ was analysed (figure 23 right). In this case the expected maximum at 1402 MeV/c^2 [14] is displaced to higher values in the mass scan. This is due to the fact that the nominal mass is at the limit of the kinematically allowed region (figure 22). For the charged $K_1(1400)$ there is again no significant indication.

The addition of K_1 amplitudes reduces the contribution of decays over the $K\pi$ S-wave (The simultaneous introduction of the $K_1(1270)$ and the $K_1(1400)$ leads to a reduction to $\approx 3\,\%$). Already for model 0 the quality of the fit does not change significantly with a removal of all $(K\pi)_s$ amplitudes. The only effect is less incoherent (phase space distributed) background. The same result was obtained for the following decays:

$$\bar{p}p(1^{--}) \xrightarrow{L=0} (K\pi)_s^\circ + \bar{K}^{*\circ} \qquad neutral \qquad (22)$$

$$\bar{p}p(1^{--}) \xrightarrow{L=0} (K\pi)_s^\pm + K^{*\mp} \qquad charged \qquad (23)$$